Chapter 19

Composition Factors Affecting the Physical Properties of Hydrophilic Zein Films

Nicholas Parris, David R. Coffin, Leland C. Dickey, and James C. Craig

Eastern Regional Research Center, U.S. Department of Agriculture*, Agricultural Research Service, 600 E. Mermaid Lane, Wyndmoor, PA 19038

Agriculturally derived alternatives to polyolefin packaging materials currently used by the food industry provide an opportunity to strengthen the agricultural economy and reduce imports of petroleum and petroleum products. Recently, considerable research has been reported on the preparation and evaluation of biopolymer films derived from renewable resources to replace petroleum-based packaging material (1–4). Most films used as packaging materials protect water-sensitive food and materials. Hence, it is important that such wrappings effectively protect against water vapor loss or gain. Zein is a hydrophobic, alcohol-soluble protein extracted from corn or corn gluten. Industrially useful zein forms tough films and coatings that resist water vapor penetration. Zein films are generally too brittle and exhibit tensile strength too low for most commercial applications. The elongation values of zein films improve significantly when plasticized with poly(ethylene glycol) (5). Cross-linking increases the tensile strength of zein films (6) and the breaking tenacity of zein fiber (7). The objective of the work described in this chapter is to study the composition of zein and measure the effect of film composition on some strength and water transmission properties of poured zein films.

Experimental

Materials

Zein isolate was obtained by ethanol extraction of dry milled corn (8); OptaZein, OZP92001 was from Opta Food Ingredients, Inc (Bedford, MA); and Zein, F-4000 was from Freeman Industries (Tuckahoe, NY). Glycerol, 95+% (GLY); poly(ethylene glycol), average MW *ca.* 400 (PEG); and 1,2,3,4-butanetetracarboxylic acid, 99% (BTCA), were obtained from Aldrich Chemical Co., Inc. (Milwaukee, Wisconsin). Poly(propylene glycol), MW 400 (PPG), was from Polysciences, Inc. (Warrington, Pennsylvania). Epichlorohydrin, formaldehyde (37% solution), glutaraldehyde (Grade I, 50% solution), and polymeric dialdehyde starch (PDS) were obtained from Sigma Chemical Co. (St. Louis, Missouri), and citric acid (CA), monohydrate, was from J.T. Baker Chemical Co. (Phillipsburg, New Jersey).

*Reference to a brand or firm name does not constitute endorsement by the U.S. Department of Agriculture over others of a similar nature not mentioned.

Methods

Chromatography. The RP-HPLC method used to separate the corn protein has been described elsewhere (8–10). Commercial and isolated zein samples, 24 mg, were dissolved in 2 mL aqueous 70% ethanol, 5% 2-mercaptoethanol (2-ME), and 0.5% sodium acetate, then vortexed at room temperature. The extracted proteins were diluted 1:10 with aqueous 55% isopropanol 5% 2-ME, separated on a Vydac (Hesperia, California) RP-C18, 5μ, 300Å, analytical column (25 × 4.6 mm) using an aqueous 0.1% trifluoroacetic acid–acetonitrile gradient at 1.0 mL/min, 55°C, and monitored at 210 nm.

Capillary Electrophoresis (CE). All CE analyses (11) were performed on a BioFocus Capillary Electrophoresis System using the CE-SDS Protein Analysis Kit from Bio-Rad Laboratories (Hercules, California). Dried protein extracts (2.0–6.0 mg) were solubilized in 1 mL of the sample buffer. Separations were performed using an uncoated fused silica capillary (24 cm × 75 μm i.d.) at 15 kV for 15 min and 20°C. Samples were injected at 10 kV for 5 s (electrophoretically), and protein was detected at 220 nm. Molecular weight standards (Bio-Rad, Hercules, California) and their corresponding molecular weights were as follows: lysozyme, 14,400; trypsin inhibitor, 21,500; carbonic anhydrase, 31,000; ovalbumin, 45,000; serum albumin, 66,200; phosphorylase B, 97,000; β-galactosidase, 116,000; and myosin, 200,000.

Film Formation. A total of 1.0 g of corn zein and plasticizer in various proportions was dissolved in 10 mL of aqueous 80% ethanol or aqueous 70% acetone, to yield a 10% mixture (12). After adding the cross-linking agent, the mixture was heated at 70°C for 30 min in 20-mL autoclave bottles. The solutions were transferred to petri dishes and then dried in a vacuum oven (33.75 kPa) at 40 or 60°C for acetone or ethanol, respectively. The dried films were stored in a desiccator at 52% relative humidity (RH) until they were tested.

Film Thickness Measurements. A micrometer (Tunico, St. James, Minnesota) was used to measure film thickness. Measured thicknesses are the mean values of 10 random placed measurements.

Water Vapor Permeability (WVP) Determination. The apparatus and methodology are described in ASTM E96-80 (13) "Water method," as modified by McHugh et al. (14). Four replicates of each film type were sealed on acrylic plastic cups and tested at 30 ± 2°C (12).

Tensile Property Measurements. Tensile properties were determined using an Instron model 1122 tensile tester with a 2000 g load cell (12). Samples were conditioned overnight in a desiccator held at 52% RH until just prior to placement in the tensile tester jaws. Tensile strength measurement data were collected and analyzed using the DOS-based Series IX, Version 6, Instron software.

Statistical Analysis. The Bonferroni LSD multiple comparison method was used for analysis of variance of the mechanical properties and WVP values. Means with no letter in common are significant at $p < 0.05$ (15).

Results and Discussion

Composition of Corn Zein

Commercially, zein is extracted from corn gluten meal, a product of corn wet milling. The zein is extracted at about 60°C with aqueous 88% isopropyl alcohol containing 0.25% NaOH (16). Less than half of the protein in the meal is isolated at low temperatures after the supernatant is decanted. Quantitative extraction of zein using aqueous ethanol from the endosperm of corn kernels on a laboratory scale has been reported (9). Zein also has been isolated from dry-milled corn, previously rinsed in a hydrocyclone to improve the extractability of its zein (8). Comparison of chromatographic profiles of the alcohol-soluble protein in commercial zein and the sample isolate extracted here from dry-milled corn, as shown in Figs. 19.1(a) and (b), shows that the isolate contained a greater number of resolved peaks compared to the commercial product. The broader, poorly resolved peaks have been attributed to deamidation of the glutamine residues of the protein in commercial zein under alkaline conditions (16). Early-eluting peaks (10–17 min) in the chromatographic profile from the zein isolate, Fig. 19.1(b), represent the β- and γ-zeins and are not present in commercial zein. These subunits reportedly contribute to the known lipid antioxidant activity of corn zein (17). Loss of this antioxidant activity appears to be linked to deamidation-induced fragmentation of corn zein resulting from hydrolysis during gluten extraction (18). The major part of the antioxidative effect of zein can be attributed to its ability to bury unsaturated lipid in the inter-or intramolecular hydrophobic spaces, where the amide groups are intimately protected from oxidative species in the aqueous environment. Later-eluting peaks (25–50 min) represent the α-zeins, which are more hydrophobic and constitute the major storage protein fraction.

The average molecular weight of native zein, determined by analytical ultracentrifugation, is 45 kDa (19). Disruption of its disulfide bonds results in two fragments with molecular weights about 19 and 22 kDa, the size of the α-zein molecules. Before wet milling, corn is steeped in an SO_2 solution, which acts as a reducing agent and cleaves protein disulfide bonds. Using capillary electrophoresis with sodium dodecyl sulfate (CE-SDS), we determined the electropherogram of zein isolate; it consisted of two partially resolved α-zein proteins with migration times of 6.2 and 6.4 min, shown in Fig. 19.2(a). The α-zeins are a complex group of closely related prolamines with molecular weights of 19 and 22 kDa (19). Estimation of their molecular weights relative to the migration times of protein standards indicated that the molecular weights of the α-zeins were 21 and 24 kDa. Commercial deflavored and decolored zein, prepared from corn gluten and subjected to a combination of alkaline treatment and alcohol washing at elevated temperature, contains adducts of the α-zeins (20). In addition to the monomers, the electropherogram of commercial zein,

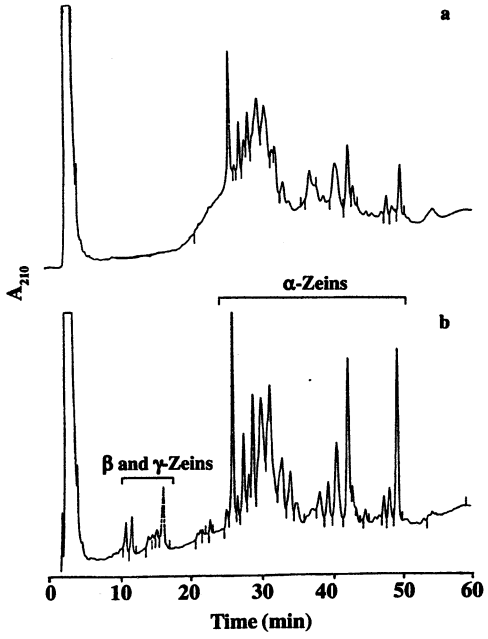

Fig. 19.1. RP-HPLC separation of alcohol-soluble zein proteins: (a) commercial zein; (b) zein isolate.

shown in Fig. 19.2(b), contained two groups of peaks with migration times of 7.5 and 8.6 min, which appear to be the dimer and tetramer of the α-zeins with molecular weights of about 45 and 85 kDa. These polymers and other higher-molecular-weight polymers at 9.5 and 10.0 min may associate primarily through disulfide linkages, since only the monomers were present after reduction with 2-mercaptoethanol, as shown in Fig. 19.2(c). Small peaks present in reduced zein samples before and after the α-zeins are probably albumins, globulins (5 min), and glutelins (7.5 min), based on SDS-PAGE assignments (21).

Tensile Properties of Zein Films

The strength and flexibility of the zein film is described by its *tensile strength* (TS) and *elongation to break* (ETB). *Initial modulus* is a measure of resistance to stretching, or the stiffness of the film. Transparent unplasticized zein films were cast from aqueous ethanol and acetone solutions. Films cast from acetone were stronger and stiffer but less elastic than those prepared from ethanol, as indicated in Table 19.1. Yamada et al. (6) reported that zein films cast from aqueous acetone solution showed

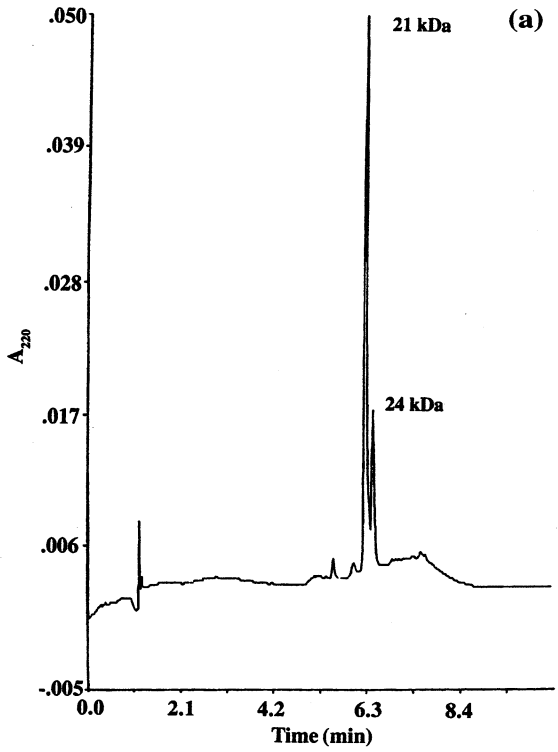

Fig. 19.2. CE-SDS of zein proteins: (a) zein isolate;

breaking strength equivalent to commercial thin plastic used for food packaging. Regardless of the solvent used to prepare these films, they were too brittle for most applications and required the addition of plasticizer to obtain adequate flexibility.

Up to 30% glycerol (GLY) could be incorporated into zein films with no significant decrease in TS; however, flexibility was not improved over unplasticized films, as indicated by their ETB values (Table 19.2). Films prepared with poly(ethylene glycol) (PEG) were more flexible than GLY-plasticized films, with little significant difference in TS compared to GLY. This could be attributed to the hydrophobic nature of the zein film matrix. However, films prepared with the more hydrophobic plasticizer, poly(propylene glycol) (PPG), were brittle with poor elongation (Table 19.2). Significant improvement in zein film flexibility, however, was achieved with blends of GLY and PPG. Films containing a GLY:PPG ratio of 1:3 exhibited ETB values almost 50 times greater than GLY-plasticized films (Table 19.2). A similar increase in elongation was not observed when PEG replaced PPG in the plasticizer

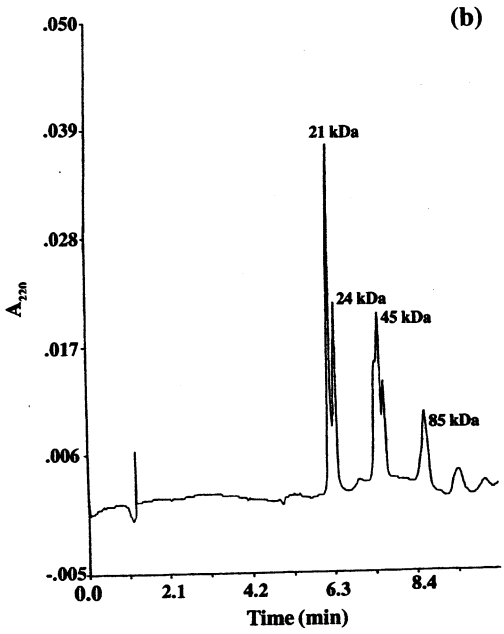

Fig. 19.2. CE-SDS of zein proteins: (b) commercial zein (OptaZein);

blend, indicating that the methyl side chain of PPG contributed to the improved film elongation. This change in plasticizer composition resulted in correspondingly small changes in TS values.

Yang et al. (7) suggested that zein fibers are brittle and exhibit poor breaking tenacity because the zein proteins are unable to unfold in alcoholic solutions, thus preventing the polypeptide chains from aligning in an ordered structure as the solvent evaporates. Incorporation of cross-linking agents into zein films raised TS values two- to threefold (Table 19.3). The modulus values indicate that these films were stiffer than the control. Films cross-linked with CA and BTCA exhibited TS values that were greater than those of the control as well as modulus values that were significantly lower than those of films made with other cross-linking agents (Table 19.3). Cross-linked films prepared in 70% acetone had TS values lower than the control and in most cases were too brittle to test (not shown).

In order to improve the flexibility of cross-linked zein films, plasticizers were incorporated at concentrations that would not impart a greasy appearance or feel to the films. Table 19.4 compares the effect of plasticizer on the tensile properties of zein films with and without glutaraldehyde cross-linking. Although all five cross-linking agents listed in Table 19.3 were evaluated, only films cross-linked with glutaraldehyde, which gave results typical of the plasticizer effect, are reported in Table 19.4. The TS value for the cross-linked films prepared with the blend of plas-

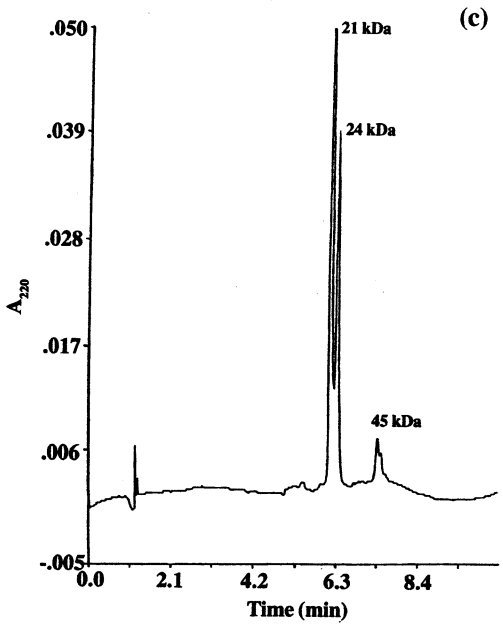

Fig. 19.2. CE-SDS of zein proteins: (c) commercial zein reduced with 2-mercaptoethanol.

TABLE 19.1
Tensile Properties of Unplasticized Zein Films Cast from Two Solvents

Solvent (aqueous)	TS	ETB (%)	Modulus (MPa)
80% ethanol	10.9b ± 1.0	3.4a ± 0.8	551b ± 66
70% acetone	14.4a ± 1.5	1.5b ± 0.3	1273a ± 57

TABLE 19.2
Effect of Plasticizer on Tensile Properties of Zein Films[a]

Plasticizer (30%)	TS (MPa)	ETB (%)	Modulus (MPa)
Control	10.9a ± 1.0	3.4c ± 0.8	551a ± 66
GLY	7.0bc ± 1.8	2.6c ± 0.4	498a ± 36
PEG	5.7c ± 1.8	44.4b ± 25.3	199b ± 82
PPG	9.4ab ± 3.7	2.8c ± 1.2	608a ± 112
GLY:PPG[b]	5.1c ± 0.9	117.8a ± 40.1	135b ± 29
GLY:PEG[b]	4.9c ± 0.5	26.6bc ± 10.5	180b ± 26

[a]Films were prepared in aqueous 80% ethanol.

[b]The ratio of plasticizers GLY:PPG or GLY:PEG was 1:3.

TABLE 19.3
Effect of Cross-Linking Agent on Zein Film Tensile Properties[a]

Cross-Linking Agent	TS (MPa)	ETB (%)	Modulus (MPa)
Control[b]	10.9c ± 1.0	3.4ab ± 0.8	551b ± 66
Formaldehyde	28.9a ± 2.6	2.4b ± 0.2	1230a ± 109
Glutaraldehyde	21.4ab ± 0.7	4.1a ± 1.4	1085a ± 42
Epichlorohydrin	19.5b ± 6.4	2.1b ± 0.3	1230a ± 110
CA	16.1bc ± 3.9	2.8ab ± 0.4	633bc ± 122
BTCA	19.1b ± 4.2	3.4ab ± 0.7	780b ± 141

[a]Films prepared in aqueous 80% ethanol.

[b]Films not cross-linked.

ticizer was lower than those of films containing the single plasticizers (GLY or PEG). ETB values for the control and cross-linked zein films were significantly greater for films containing 30% GLY/PPG compared to 15% GLY or PEG.

Clear zein films cross-linked with up to 20% polymeric dialdehyde starch (PDS) exhibited higher TS and modulus values than the control (Table 19.5). Zein-PDS films containing 15% GLY had slightly lower TS values, and the initial modulus was approximately half that of the cross-linked unplasticized zein films.

Water Vapor Barrier Properties (WVP)

The effect of cross-linking agent, plasticizer, and preparation solvent on water vapor permeability are shown in Table 19.6. Lowest WVP values were obtained for unplasticized zein films. Of these, films cross-linked with 20% PDS exhibited the best water barrier properties. Films prepared in acetone appeared to have lower WVP values than those prepared in ethanol. Incorporation of plasticizer into zein films almost doubled WVP values. Decreasing the ratio of GLY:PPG in zein films from 3:1 to 1:1 and 1:3 decreased their WVP values (Fig. 19.3). The variation in WVP

TABLE 19.4
Effect of Plasticizer on Film Tensile Properties of Cross-Linked Zein Films[a]

Cross-Linking Agent	Plasticizer	TS (MPa)	ETB (%)	Modulus (MPa)
Control[b]				
	15% GLY	5.2a ± 0.7	4.4b ± 0.5	499a ± 76
	15% PEG	4.3a ± 1.4	3.4b ± 1.5	323b ± 82
	30% GLY:PPG[c]	5.1a ± 0.9	117.8a ± 40.1	135c ± 29
Glutaraldehyde				
	15% GLY	19.8a ± 0.9	3.0b ± 0.5	412a ± 64
	15% PEG	10.4b ± 2.0	2.8b ± 0.2	397a ± 76
	30% GLY:PPG[c]	1.4c ± 0.1	224.0a ± 30.9	25b ± 11

[a]Films were prepared in aqueous 80% ethanol.

[b]Films not cross-linked.

[c]The ratio of plasticizers GLY:PPG was 1:3.

TABLE 19.5
Tensile Properties of Zein–Dialdehyde Starch Cross-Linked Films[a]

Dialdehyde Starch (%)	TS (MPA)	ETB (%)	Modulus (MPA)
0	10.9a ± 1.0	3.4a ±0.8	551c ± 66
5	15.8a ± 5.0	1.9b ± 1.0	1074ab ± 133
10	17.5a ± 3.1	1.7b ± 0.2	1145ab ± 100
15	13.6a ± 6.6	1.8b ± 0.2	919b ± 89
20	17.1a ± 3.2	1.8b ± 0.3	1213a ± 148
20[b]	13.5a ± 4.0	2.6ab ± 0.3	569c ± 105

[a]Films were preparted in aqueous 80% ethanol.

[b]Films contained 15% GLY.

TABLE 19.6
Water Vapor Permeability of Zein Films

Film Type	Solvent	Plasticizer	WVP (g mm/kPa hm^2)
Zein	Ethanol	None	0.620c ± 0.036
Zein	Acetone	None	0.577c ± 0.009
Zein	Ethanol	GLY:PPG (30%)[a]	1.060ab ± 0.032
Zein	Acetone	GLY (15%)	1.010b ± 0.108
Zein/PDS (20%)	Ethanol	None	0.533c ± 0.031
Zein/PDS (20%)	Ethanol	GLY:PPC (30%)[a]	1.015a ± 0.100

[a]The ratio of mixed plasticizers was 1:3.

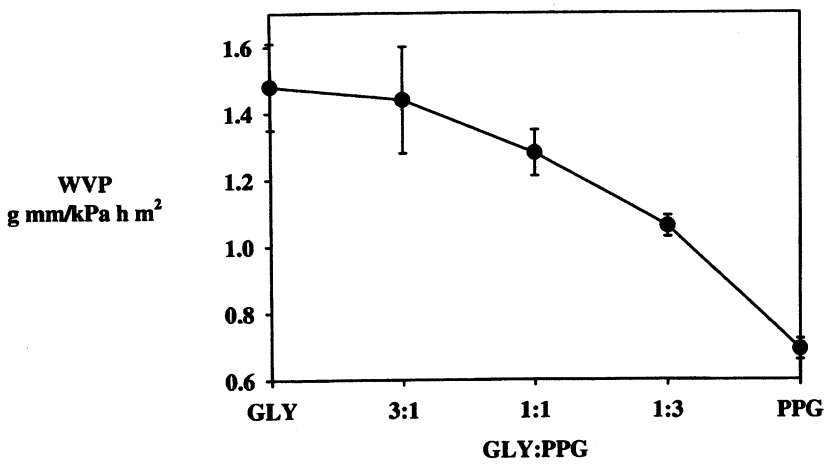

Fig. 19.3. Effect of PPG concentration on zein film water vapor permeability.

values between zein films with the same plasticizer composition also decreased with increasing PPG concentration. These results could be attributed to preferential separation GLY over PPG from the film.

Armed with this information on the compositional factors affecting the tensile and water vapor barrier of hydrophilic zein films, future research will be directed toward investigating the potential of zein as a coating for recyclable cellulosic material using both commercial zein preparations and the extracted zein isolate.

Acknowledgment

We thank Dr. John G. Phillips for the statistical analysis of variance of the mechanical properties and WVP values.

References

1. Park, J.H., and M.S. Chinnan, *Properties of Edible Coatings for Fruits and Vegetables,* ASAE Paper No. 90-6510, American Society of Agriculture Engineers, St. Joseph, Michigan, 1990.
2. Aydt, T.P., C.L. Weller, and R.F. Testin, Mechanical and Barrier Properties of Edible Corn and Wheat Protein Films, *Trans. ASAE 34:* 207 (1991).
3. Gennadios, A., C.L. Weller, and R.F. Testin, Temperature Effect of Oxygen Permeability of Edible Protein-Based Films, *J. Food Sci. 58:* 212 (1993).
4. Gennadios, A., and C.L. Weller, Moisture Adsorption by Grain Protein Films, *Trans. ASAE 37:* 535 (1994).
5. Park, H.J., J.M. Bunn, C.L. Weller, P.J. Vergano, and R.F. Testin, Water Vapor Permeability and Mechanical Properties of Grain Protein-Based Films as Affected by Mixtures of Polyethylene Glycol and Glycerin Plasticizers, *Trans. ASAE 37:* 1281 (1994).
6. Yamada, K., H. Takahashi, and A. Noguchi, Improved Water Resistance in Edible Zein Films and Composites for Biodegradable Food Packaging, *Int. J. Food Sci. Technol. 30:* 599 (1995).
7. Yang, Y, L. Wang, and S. Li. Formaldehyde-Free Zein Fiber Preparation and Investigation, *J. Appl. Polym. Sci. 59:* 433 (1996).
8. Parris, N., L.C. Dickey, M.J. Kurantz, R.O. Moten, and J.C. Craig, Water Vapor Permeability and Solubility of Zein/Starch Hydrophilic Films Prepared from Dry Milled Corn Extract, *J. Food Eng.,* accepted (1997).
9. Wilson, C.M., Multiple Zeins from Maize Endosperms Characterized by Reversed-Phase High Performance Liquid Chromatography, *Plant Physiol. 95:* 777 (1991).
10. Dombrink-Kurtzman, M.A., Examination of Opaque Mutants of Maize by Reversed-Phase High-Performance Liquid Chromatography and Scanning Electron Microscopy, *J. Cereal Sci. 195:* 57 (1994).
11. Parris, N., L.C. Dickey, and J.C. Craig, Quantitative Analysis of Corn Zein by Capillary Electrophoresis, *J. Cereal Chem. 74:* 766–770 (1997).
12. Parris, N., and D.R. Coffin, Composition Factor Affecting the Water Vapor Permeability and Tensile Properties of Hydrophilic Zein Films, *J. Agric. Food Chem. 45*(5): 1596 (1997).
13. ASTM. Standard Test Method for Water Vapor Transmission of Materials, *ASTM Book of Standards,* American Society for Testing and Materials, Philadelphia, 1980, p. E96-80.

14. McHugh, T.H., R. Avena-Bustillos, and J.M. Krochta. Hydrophilic Edible Film: Modified Procedure for Water Vapor Permeability and Explanation of Thickness Effects, *J. Food Sci. 58:* 899 (1993).
15. Miller, R.G., Jr., *Simultaneous Statistical Inference,* 2nd edn., Springer-Verlag, New York–Heidelberg–Berlin, 1981, pp. 67–70.
16. Reiners, R.A., J.S. Wall, and G.E. Inglett, in *Industrial Uses of Cereals,* edited by Y. Pomeranz, American Association of Cereal Chemists, Inc., St. Paul, Minnesota, 1973, pp. 285–302.
17. Matsumura, Y., P.P. Andonova, Y. Hayashi, H. Murakami, and T. Mori, Antioxidant Activities of Zeins from Different Maize Varieties against Docosahexaenoic Acid Ethyl Ester, *Cereal Chem. 71:* 428 (1994).
18. Chiue H., T. Kusano, and K. Iwami, Deamidation-Induced Fragmentation of Maize Zein and Its Linked Reduction in Fatty Acid-Binding Capacity as well as Antioxidative Effect, *Food Chem. 58:* 111 (1997).
19. Turner, J.E., J.E. Boundy, and R.J. Dimler, Zein: A Heterogeneous Protein Containing Disulfide-Linked Aggregates, *Cereal Chem. 42:* 452 (1965).
20. Cook R.B., F.M. Mallee, and M.L. Shulman, U.S. Patent 5,254,673 (1993).
21. Wallace, J.C., M.A. Lopes, E. Paiva, and B.A. Larkins. New Methods for Extraction and Quantitation of Zeins Reveal a High Content of γ-Zein in Modified opaque-2 Maize, *Plant Physiol. 92:* 191 (1990).

In vivo studies on the nuclear behavior of the arbuscular mycorrhizal fungus *Gigaspora rosea* grown under axenic conditions

B. Bago[1,*], W. Zipfel[2], R. M. Williams[2], H. Chamberland[3], J. G. Lafontaine[3], W. W. Webb[2], and Y. Piché[1]

Summary. The distribution and fate of nuclei of the arbuscular-mycorrhizal fungus *Gigaspora rosea* during late stages of axenic cultures were studied in fixed cultures by transmitted light, conventional and confocal laser scanning microscopy, and in live cultures with two-photon fluorescence microscopy. Mature specimens not yet showing apical septation displayed oval-shaped nuclei localized in lateral positions of the hypha all along the germ-tube length. Beside these, round-shaped nuclei were found to migrate along the central germ-tube core. Some (rare) germ-tube areas, delimited by septa and containing irregularly shaped, much brighter fluorescent nuclei were also found. Specimens that had just initiated the septation process after germ-tube growth arrest displayed round or oval-shaped nuclei in several portions of the germ tubes. These hyphal areas often alternated with other septa-delimited cytoplasmic clusters which contained distorted, brightly fluorescent nuclei. Completely septated specimens mostly lacked nuclei along their germ tubes. However, highly fluorescent chromatin masses appeared within remnants of cytoplasmic material, often compressed between close septa. Our results provide a first clear picture of the in vivo distribution of nuclei along arbuscular mycorrhizal fungal germ tubes issued from resting spores, and suggest that selective areas of their coenocytic hyphae are under specific, single nuclear control. They indicate as well that random autolytic processes occur along senescing *G. rosea* germ tubes, probably as a consequence of the absence of a host root signal for mycorrhizal formation. Finally, the data presented here allow us to envisage the fate of nuclei released by the germinating spore after nonsymbiotic fungal growth arrest.

Keywords: Arbuscular-mycorrhizal fungi; Axenic culture; DAPI; *Gigaspora rosea*; Multiphoton microscopy; Nuclei.

*Correspondence and reprints (present address): Plant and Soil Biophysics Laboratory, Eastern Regional Research Center, ARS, U.S. Department of Agriculture, 600 E. Mermaid Lane, Wyndmoor, PA 19038, U.S.A.

Abbreviations: AM fungi arbuscular-mycorrhizal fungi; DAPI 4′,6-diamidino-2-phenylindole; FM fluorescence microscopy; CLSM confocal laser scanning microscopy; 2PM two-photon microscopy; PI propidium iodide; PMT photomultiplier tube.

Introduction

Arbuscular mycorrhizal fungi (AM fungi; Glomales, Zygomycota) colonize roots of most land plants to form arbuscular mycorrhizas (Smith and Read 1997). The ecological and economical importance of this symbiosis has led to an increased interest in the study of this biotrophic association from which both partners benefit (Azcón-Aguilar and Bago 1994, Barea and Jeffries 1995). One of the major difficulties of such studies is the inability of the AM fungi to fulfill their life cycle in the absence of a host root, which has led to their classification as obligate symbionts (Azcón-Aguilar and Barea 1994).

When axenically cultured, the AM fungal spore germinates and its thick-walled germ tube extends in the culture medium, occasionally forming right-angled branches. Under these conditions, development can be maintained up to 2–4 weeks (depending on the fungal species, growth medium, and spore age), and the germ tube can reach several centimeters in length. If the fungus does not find a host root to colonize, apical septation and cytoplasm retraction have been reported to occur (Mosse 1962, 1988; Hepper 1983; Bonfante and Bianciotto 1995; Bonfante and Perotto 1995). At the end of this process the whole germ tube appears

septated and empty (Hepper 1983, Mosse 1988), and the spore enters a new dormancy state (Giovannetti et al. 1994, Bonfante and Bianciotto 1995). The cessation of growth is not understood but is probably not due to the exhaustion of any essential component of the parent spore that is able to re-germinate several times (Hepper 1984, Bago 1990). Since the early studies by Gerdemann (1955) and Mosse (1959), all attempts to supply the fungus axenically with the necessary "factor(s)" to overcome its obligatory condition have failed, even though AM fungal spores were found to contain the metabolic machinery necessary to sustain vegetative hyphal growth (reviewed by Hepper 1984, Azcón-Aguilar and Barea 1994). The requirement of a "switch on" signal by the host plant to start the fungal metabolism after symbiosis establishment has been proposed to explain the failure of AM fungi to grow in a free-living status (Becard and Piché 1989, Bago et al. 1996). The nature of this "switch on" signal still remains unknown, as are the cytological processes leading to the complete fungal growth arrest when such a signal is lacking.

Similar to other members of Zygomycota, AM fungi are coenocytic and multinucleated (Bianciotto and Bonfante 1992 and references therein). Different cytological studies have been carried out on the nuclear status of AM fungal spores (Sward 1981a, b; Cooke et al. 1987; Burggraaf and Beringer 1989; Bianciotto and Bonfante 1992; Bécard and Pfeffer 1993) and hyphae, both before (Sward 1981c, Cooke et al. 1987, Meier and Charvat 1992, Bianciotto and Bonfante 1993) and after (Bonfante-Fasolo et al. 1987, Bianciotto and Bonfante 1992, Balestrini et al. 1992) symbiosis establishment. Dormant AM fungal spores have been estimated to contain between 1,700 to 20,000 nuclei, depending on the fungal species and the quantification method used (Cooke et al. 1987, Burggraaf and Beringer 1989, Bécard and Pfeffer 1993). When the spore germinates, nuclei migrate into the emerging germ tube (Sward 1981b). Actively-growing germ tubes typically do not contain nuclei 5–20 μm from the apex (Sward 1981c, Cooke et al. 1987). Along the remaining hypha the nuclei display round or oval shapes, dispersed chromatin and a conspicuous nucleolus (Bianciotto and Bonfante 1992). Observations on fixed specimens indicated that nuclei were linearly distributed at a constant density of approx. 460/cm (Bécard and Pfeffer 1993), appearing frequently associated in groups of 2 or 3–4 (Cooke et al. 1987, Bianciotto and Bonfante 1993). Previously it has been reported that AM fungi do not synthesize DNA in the absence of AM formation (Burggraaf and Beringer 1989, Viera and Glenn 1990). More recently, however, DNA synthesis has been confirmed by bromodeoxyuridine incorporation tests (Bianciotto and Bonfante 1993). Results obtained with fluorescence microscopy and image analyses also led Bécard and Pfeffer (1993) to conclude that nuclear division and DNA replication do occur nonsymbiotically in AM fungi.

Apart from the above observations, little is known about the actual role and behavior of the some 800 nuclei released from the AM fungal spore (Bécard and Pfeffer 1993) after germination. This is specially true when considering the final stages of axenic development, when the fungus has proved unable to find a host root to establish symbiosis with and stops growing. The current knowledge on this particular issue could be summarized by these two observations: (i) Mosse (1988), in a review on different aspects of the "independent" growth of AM fungi, presented two photographs of earlier unpublished results in which aceto-carmine stained nuclei of old *Glomus mosseae* axenic hyphae displayed distorted shapes compared to nuclei in young, similarly stained germ tubes; (ii) Cooke et al. (1987) reported that old, septated hyphae showed little or no cellular content and lacked nuclei. However, several fundamental questions still remain unanswered: How do nuclei distribute along, and control the long, coenocytic fungal germ tube? What is their behavior after assessment of symbiosis failure? What is their final fate: are they "reabsorbed" through cytoplasmic retraction by the spore which released them, or, on the contrary, discarded and destroyed? The answer to these questions could further clarify the mechanisms leading to fungal growth arrest under axenic conditions.

The recent development of multi-photon microscopy (Denk et al. 1990, 1995; Williams et al. 1994; Xu et al. 1996; Xu and Webb 1996) has opened new prospects in cell-cycle studies on living specimens. Due to the relatively lower level of damage induced by this technique on living tissues, especially when using UV-absorbing fluorophores, experiments can now be conducted over longer periods of time (Williams et al. 1994, Denk et al. 1995). The aim of the present work was to study the behavior of nuclei of the AM fungus *Gigaspora rosea* in vivo during its nonsymbiotic phase by combining the use of the UV-absorbing fluorochrome 4′,6-diamidino-2-phenylindole (DAPI) with 2-photon microscopy (2PM). Three particular points will be addressed: (i) nuclear distrib-

ution along the growing germ tubes; (ii) behavior of fungal nuclei during axenic growth cessation processes; (ii) fate of released nuclei after failure of AM symbiosis establishment.

Material and methods

Biological material

Spores of *Gigaspora rosea* Nicolson & Schenk (formerly considered *G. margarita*, Bago et al. 1998) (DAOM 194757, Biosystematic Research Centre, Ottawa, Canada) were collected from pot cultures by the wet sieving and decantation technique (Gerdemann and Nicolson 1963) and surface-sterilized (Mosse 1962).

Observations on fixed specimens

Spores were cultured (25 °C in the dark) in petri dishes (9 cm diameter) containing 20 ml of an autoclaved (121 °C, 20 min) water-agar medium (0.8% Bacto-Difco agar in distilled water). A minimum of 5 days after germination, ten specimens were fixed (10% formalin in distilled water, 1 h) and carefully transferred with a Pasteur pipette to microscope slides. Specimens were then stained with propidium iodide (PI; Sigma, St. Louis, Mo., U.S.A.; 5 μg/ml), or DAPI (Sigma; 25 μg/ml) (Heath, 1987). Observations by conventional fluorescence microscopy (FM) were carried out with a Reichert Polyvar instrument, using either blue (PI) or UV (DAPI) illumination. Observations by laser confocal scanning microscopy (CLSM) were performed either with a Zeiss LSM-310 instrument (×100 oil immersion objective; z-axis step, 0.55 μm), using an argon laser (514 nm) on specimens stained with PI; or with an Olympus IMT-2 instrument (DApo 100UV/340, 1.3 N.A., ×100 oil immersion objective; z-axis step, 0.3 μm) on specimens stained with DAPI.

Observations on in vivo specimens

Effect of DAPI on spore germination and hyphal development

To find the most innocuous DAPI concentration for in vivo microscopic studies on *G. rosea*, preliminary viability tests were carried out. Water-agar media containing different concentrations of DAPI were prepared. The fluorochrome was first prepared as a stock solution (1 mg/ml in distilled water), then sterilized by filtration (Uniflo 13 mm, 0.2 μm pore; Schleicher and Schuell, Keene, N.H., U.S.A.). Different volumes of the sterile stock solution were added to the autoclaved (121 °C, 20 min) water-agar medium to obtain final fluorochrome concentrations of 0, 5, 12.5, and 25 μg/ml. Eight surface-sterilized spores per treatment were transferred to petri dishes (9 cm diameter) containing 20 ml of the different media. Spores were maintained in culture for 21 days at 25 °C in the dark, and in a 2% CO_2 atmosphere to enhance hyphal growth (Bécard and Piché 1989). Hyphal development was measured at the end of the assay as described by Marsh (1971) with a 2 mm side grid.

Two-photon microscopy

Spores of *G. rosea* were pre-germinated (25 °C, darkness) in water-agar medium. Germinated spores were transferred to special microscope observation chambers (chambered coverglass; NUNC InterMed, Naperville, Ill., U.S.A.) consisting of 75 × 25 mm No. 1 borosilicate coverglasses bonded to chambered upper structures with plastic removable lids. The chambers were filled with 5 ml of autoclaved water-agar medium ammended with 5 μg of DAPI per ml (filtration-sterilized). This concentration was chosen following the preliminary viability tests (see Results). Three pre-germinated spores were transferred to each chambered coverglass, a total of five replicates were prepared. Spores were cultured at 25 °C in the dark for 10 days, in a slight slope position to allow *G. rosea* germ tubes, which present a negative geotropism (Watrud et al. 1978), to grow as close as possible to the coverglass. The chambered coverglass allowed the direct, in vivo observation of *G. rosea* specimens at high magnification.

Images of DAPI-stained *G. rosea* were acquired with a two-photon laser scanning microscope. 740 nm mode-locked excitation (80 fs pulses, 80 MHz repetition rate) was obtained from an argon-pumped Ti:Sapphire laser (Tsunami, Spectra Physics, Mountain View, Calif., U.S.A.). The beam was attenuated and directed into a retrofitted Bio-Rad MRC-600 confocal scanning box aligned to an inverted microscope (Zeiss Axiovert-35) with a ×40, 1.2 N.A. water immersion objective (Zeiss). Typical illumination powers at the specimen were 5–10 mW.

Because multiphoton fluorescence excitation is intrinsically localized (Denk et al. 1990), confocal detection optics are unnecessary. To avoid signal degradation by extraneous optical elements, fluorescence detection was accomplished external to the confocal box. The fluorescence was separated from the excitation light by a 680 nm, long-pass dichroic (Chroma Technology Corp., Brattleboro, Vt., U.S.A.), spectrally filtered with a 2 mm thick BGG22 optical filter (380–530 nm) and monitored by a photomultiplier tube (PMT; Hamamatsu, Bridgewater, N.J., U.S.A.; HC 125-02) placed conjugate to the back aperture of the objective. The signal from the external PMT is sent to the external input of the MRC-600. The transmitted light images were acquired with a light pipe that delivered light through the specimen to the standard PMT's in the Bio-Rad confocal box. Each time-lapse series of images consisted of multiple (1 s) frames acquired at 30 s intervals using the macro programming language available with the Bio-Rad confocal software. Nuclear movement movie shown at the Internet's "AMF web page" (http://www.rsvs.ulaval.ca/~crbf/amf.html) were prepared using the Adobe Premiere software.

Results

Observations on fixed specimens

Both PI and DAPI staining on fixed specimens revealed similar features of shape and distribution of nuclei along fungal hyphae, so that these results are presented independently of the fluorochrome used.

Conventional FM and CLSM on *G. rosea* germ tubes confirmed earlier observations reporting the coenocytic and multinucleate nature of this AM fungus (Fig. 1). Nuclei distributed linearly along hyphae, but were absent from the apex (Fig. 1 a). The latter portion devoid of nuclei was generally less than 10 μm in length, sometimes extending to as much as 50 μm. Nuclei in the immediate vicinity of nonseptated apices were usually roundish to oval in shape, and formed groups of two, three, or four. CLSM revealed nuclei as quite heterogenously stained, often displaying a darker, central zone corresponding to the nucleolus (Fig. 1 a).

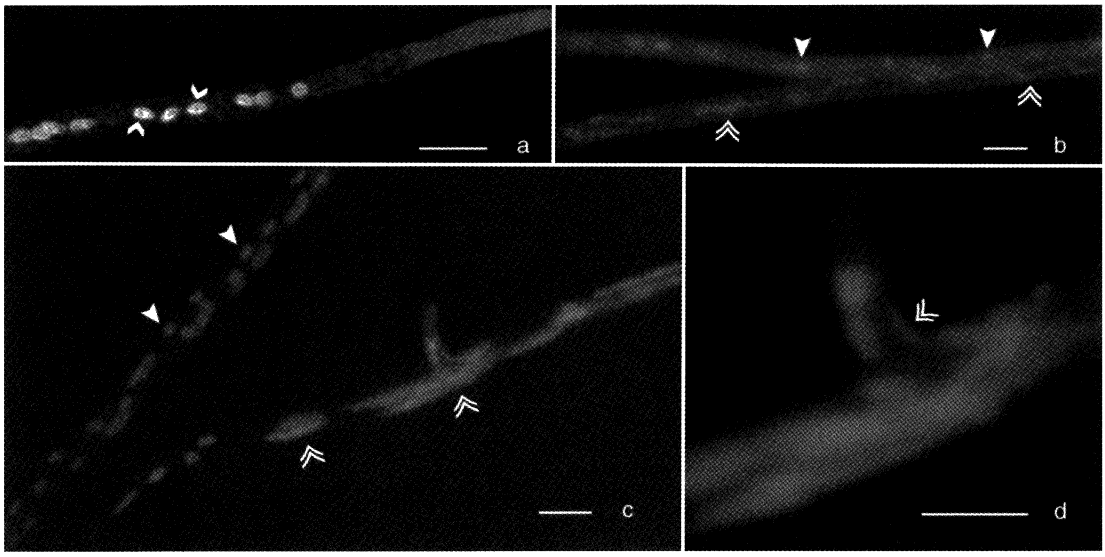

Fig. 1 a–d. Conventional fluorescence microscopy on fixed *Gigaspora rosea* specimens. **a** Apical zone of a 5-day-old germ tube stained with PI. Note the hetereogenously stained chromatin and the apparent nucleoli (arrowheads). **b** and **c** Nuclear features displayed by germ tubes central and distal portions (DAPI staining). Striking elongated and irregularly shaped nuclei (double arrowheads) coexist with more regular, round to oval nuclei (solid arrowheads). Both nuclear types appear in well-delimited hyphal portions. **d** Higher magnification of the hyphal branching portion shown in **c**. Chromatin strands (double arrowheads) extend several micrometers within the hypha. Bars: a, b, and d, 10 μm; c, 20 μm

Central and distal portions of hyphae were also multinucleated (Fig. 1 b, c). Besides the roundish or oval shape showed by nuclei in some hyphal portions, other hyphal zones displayed nuclei with irregular outlines (Fig. 1 b), as well as strands of fluorescent chromatin (Fig. 1 c). Optical sections (CLSM, z-series) of such chromatin strands confirmed that they extended several micrometers within the germ tube (Fig. 1 d).

Observations on in vivo specimens

Effect of DAPI on spore germination and hyphal development

Results on the effect of DAPI on spore germination and germ-tube development are shown in Table 1. DAPI did not influence spore germination at any of the concentrations tested. However, a significant negative effect on germ-tube development was found at concentrations of 12.5 and 25 μg/ml. At lower concentration (5 μg/ml), specimens did not show significant differences in germ-tube development compared to the nontreated specimens. This fluorochrome concentration is within the recommended range for vital staining with DAPI in culture medium (Heath 1987), and was therefore selected to carry out the in vivo experiments.

Table 1. Effect of DAPI on spore germination and hyphal development of 21-day-old axenically cultured *Gigaspora rosea* spores

	DAPI (μg/ml)			
	0.0	5.0	12.5	25.0
Spore germination (%)	62.5a[1]	50.0a	75.0a	62.5a
Hyphal development (no. of intersections)	753a	485ab	466b	313b

[1]Different letters express significant differences for $P < 0.05$ (Z statistic)

Two-photon microscopy

Three *G. rosea* specimens (A, B, and C), representative of the different developmental stages of axenically cultured germ tubes are presented. The rest (12) of the specimens studied showed features similar to one of these three.

Specimen A (Figs. 2 and 3) consisted of an axenically cultured *G. rosea* spore whose germ-tube did not yet display apical septation. A schematic representation of the nuclear distribution and features of this specimen is shown in Fig. 2 with the different studied zones framed and labeled. Transmitted-light (left) and 2PM (right) pictures of the corresponding regions are illustrated in Fig. 3 a–f.

Specimen A did not show septation or cytoplasmic retraction in its apex (Figs. 2 a and 3 a), where the

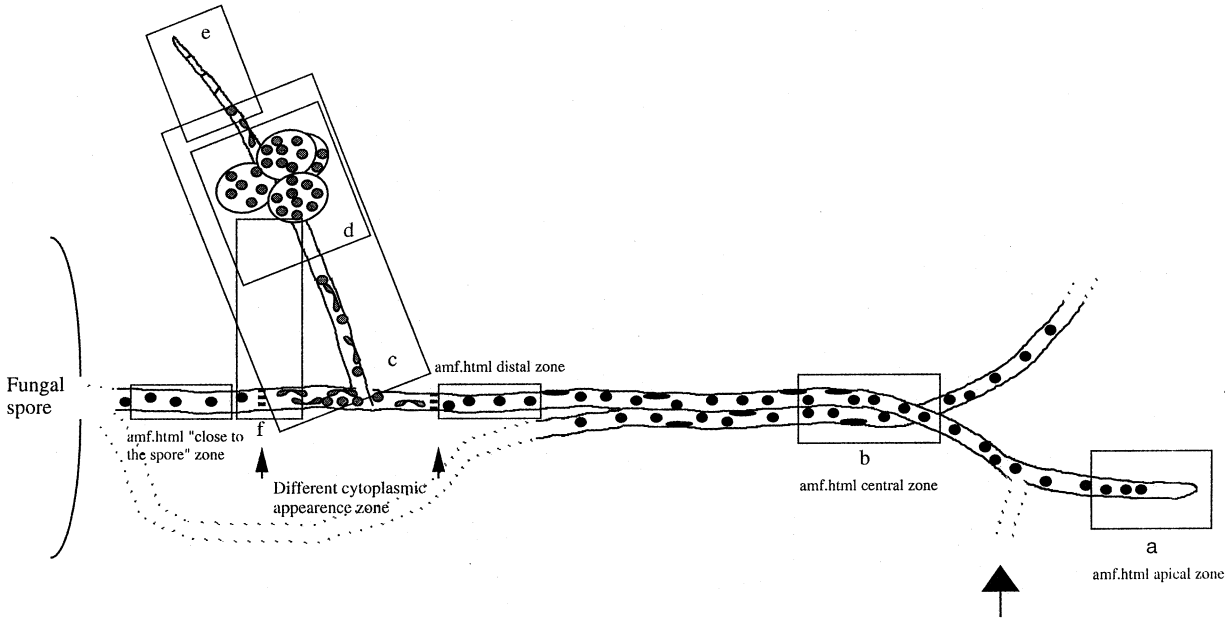

Fig. 2. Schematic representation of nuclear distribution and features along specimen A germ tubes, reconstructed from data obtained by 2PM. Black nuclei represent dim, round to oval-shaped nuclei. Grey nuclei represent irregularly shaped nuclei displaying a brighter fluorescence. *a–f* Details corresponding to Fig. 3 a–f. *amf.html* Time series presented at the AMF web page showing nuclear movement along germ tubes. The schema is not to scale

fungal cytoplasm appeared quite vacuolated (Fig. 3 a, left). 2PM revealed (Fig. 3 a, right) groups of 2–4 roundish-oval nuclei at the subapical zone (35 μm back the apex), occupying either a central or a lateral position within the hypha. Time lapse series of this apical zone (AMF web page) revealed an extremely slow, if any, cytoplasmic streaming, in which some nuclei seemed to move back from the apex towards the spore. These features were maintained along the germ tube back to the spore to the point where the first ramification occurred (Fig. 2); from this point back to the spore, a more intense cytoplasmic streaming was noted.

Several millimeters back from the first ramification and towards the spore, the principal germ tube ran together with another hypha originating from the same spore (Figs. 2 b and 3 b). It was not possible to assess if the second hypha was a ramification of the principal germ tube or another germ tube issued from a spore regermination. Both hyphae ran very close together for several millimeters and at some points their cell walls seemed to merge (Fig. 3 b, left). However, 2PM revealed that, as far as nuclei were concerned, each hypha maintained its integrity (Fig. 3 b, right). Nuclei appeared round or oval in shape, the latter usually being close to the hyphal wall, whereas the round nuclei appeared at more central locations. Time lapse series of this and other central zones (AMF web page) revealed that oval, laterally located nuclei did not usually move, whereas the more roundish ones moved along the central part of the germ tube. Nuclear movement seemed to involve cytoplasmic streaming, and depending on the germ-tube zone observed they progressed either towards the apex or towards the spore.

Closer to the spore a ramification containing a group of auxiliary cells was found (Figs. 2 and 3 c–f). Nuclei within the ramification (the auxiliary cells' subtending hypha), within the auxiliary cells and also within a restricted portion of the principal germ tube (in the proximity of the auxiliary cells' subtending hypha) were markedly brighter than the nuclei described above (Fig. 3 c). While most nuclei were roundish, a few others appeared irregularly shaped. Nuclei of auxiliary cells were round and bright (Fig. 3 d), some irregular, brightly fluorescent strands of chromatin appeared in auxiliary cells' stems (Fig. 3 d). Such chromatin strands were also present at the lower (Fig. 3 c) and upper (Fig. 3 e) parts of the auxiliary cells' subtending hypha. The apex of this subtending hypha was the only one in the whole specimen A which was septated (Fig. 3e, left). Adjacent to

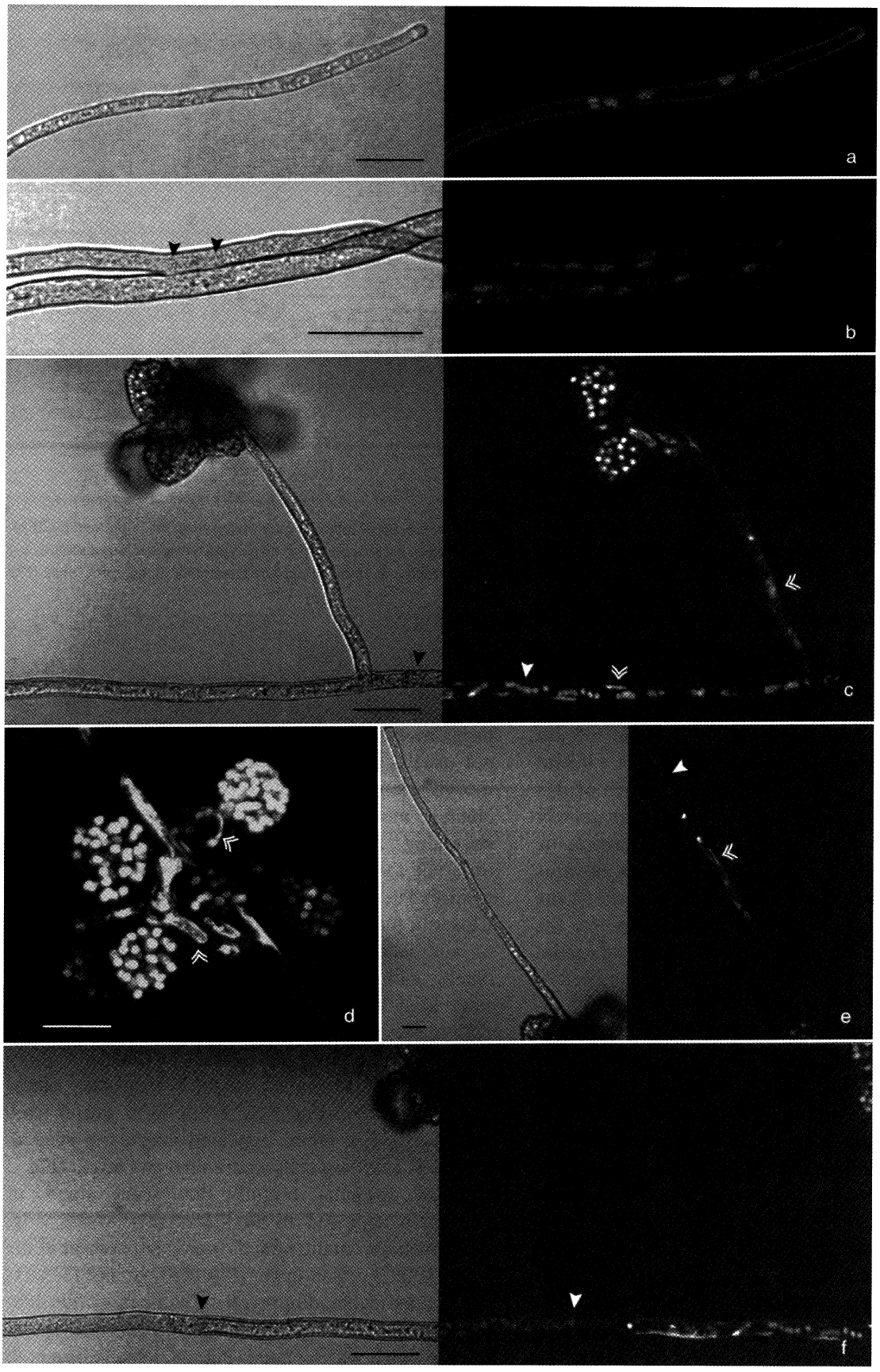
a
b
c
d
e
f

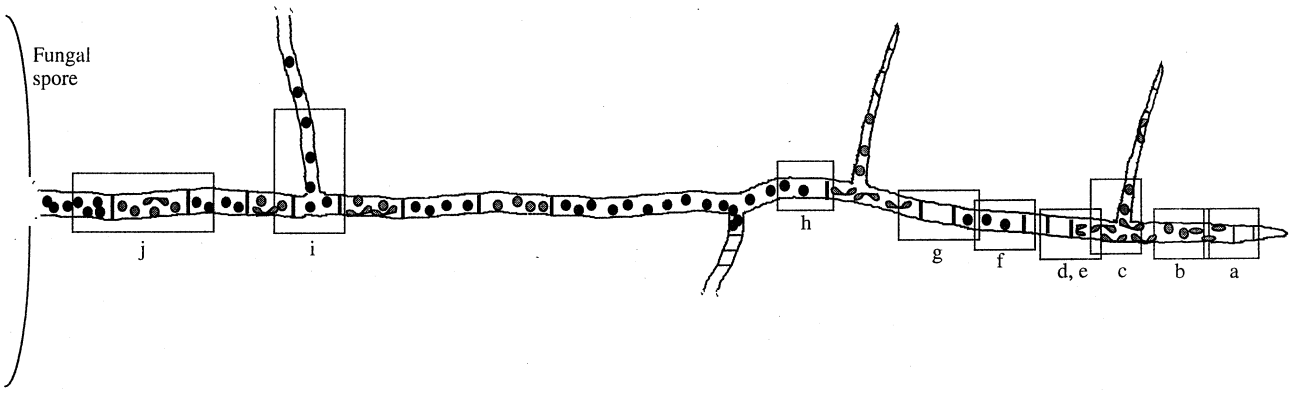

Fig. 4. Schematic representation of specimen B. Black and grey nuclei represent nuclei with similar features as in Fig. 2. *a–j* Details corresponding to Fig. 5 a–j. The schema is not to scale

the septated zone, three roundish, dim nuclei were observed (Fig. 3 e, right), followed by round bright nuclei, as well as of chromatin strands.

Initially no septa were seen in specimen A along the principal germ tube. However in the region where the auxiliary cells' subtending hypha arose a significant difference in cytoplasm appearence was noted (delimited in Figs. 2 and 3 c, f, left). Within this region, neither cytoplasmic streaming nor nuclear movement was found, but the nuclei exhibited brighter DAPI fluorescence and some of them were irregular and even strand-shaped (Fig. 3 f, right). Approximately 3 h after this initial observation two septa formed, clustering this distinct germ-tube region (not shown). Immediately behind this region the cytoplasm displayed again its normal appearance (Fig. 3 f, left) and dimmer, roundish nuclei were found (Fig. 3 f, right). These features were maintained from this region to the spore's closest germ-tube zones, where cytoplasmic and nuclear movement were faster than previously observed (AMF web page).

Specimen B (Figs. 4 and 5) consisted of a *G. rosea* germ tube whose apex had initiated septation. In the schematic representation of the specimen (Fig. 4) the different zones studied are framed and labeled. The corresponding transmitted-light and 2PM pictures are shown in Fig. 5.

Observations on this specimen revealed septated apical zones (Figs. 4 and 5 a) showing similar features to hyphal zones described by different authors (see Introduction) as "devoid of cytoplasm" (from now on, "clean septa" zones). Nuclei were seen as soon as cytoplasm was present in the germ tube (Fig. 5 a, right). Although some of these nuclei were roundish, most of them appeared irregular. Independently of their shape, all of them displayed bright fluorescence. These nuclear features were maintained throughout a germ-tube region (Figs. 4 and 5 a–d) along which cytoplasm appeared vacuolated and/or granular. Neither cytoplasmic streaming nor nuclear movement was noted. Brightly fluorescent chromatin strands were often observed.

A zone displaying "clean septa" (Figs. 4 and 5 d, upper) marked the end of the cytoplasmic area described above. Just before the first septum of this zone, a highly fluorescent mass was observed (Fig. 5 d, lower). Z-series of the region revealed that this mass was constituted mainly of chromatin strands

---

Fig. 3 a–f. In vivo , 2PM of a nonseptated, axenically cultured *G. rosea* specimen (specimen A). Transmitted-light (left) and 2PM (right) micrographs display cytoplasmic and nuclear features of different germ-tube zones. **a** Apical zone. **b** Central portion of two close-running germ tubes. In certain points cell walls seemed to merge (solid arrowheads), however, nuclei of both hyphae remained independent. **c** Germ-tube zone from which auxiliary cells originate. Both germ-tube and auxiliary cells' subtending hyphae display bright fluorescent nuclei, usually round in shape (solid arrowhead). Some bright chromatin strands are also noted (double arrowheads). **d** Higher magnification of the auxiliary cells showing their round, bright nuclei. Some chromatin strands are also evident in the auxiliary cells' stem (double arrowheads). **e** Apical zone of the auxiliary cells' subtending hyphae. Three round, dim nuclei (solid arrowhead) are followed by brighter irregular nuclei and chromatin strands (double arrowheads). **f** Along several micrometers of the germ-tube zone from which auxiliary cells originated a change in cytoplasm appearance was noted (to the black arrowhead's right) corresponding to brightly fluorescent, irregularly shaped nuclei in the fluorescent image (to the white arrowhead's right). Out of this zone nuclei remained dimmer and rounder (to the white arrowhead's left). Bars: 20 μm

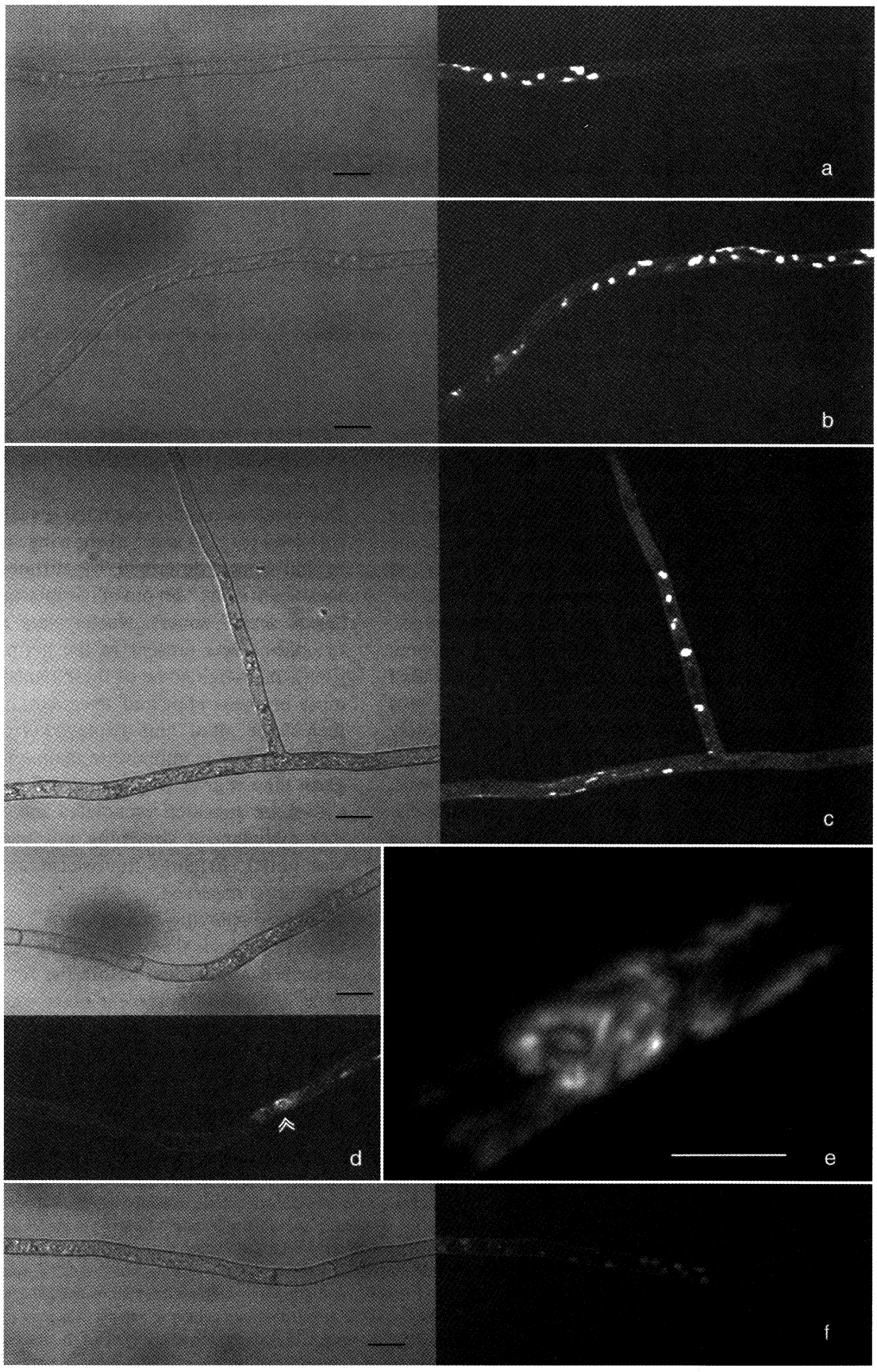
a
b
c
d
e
f

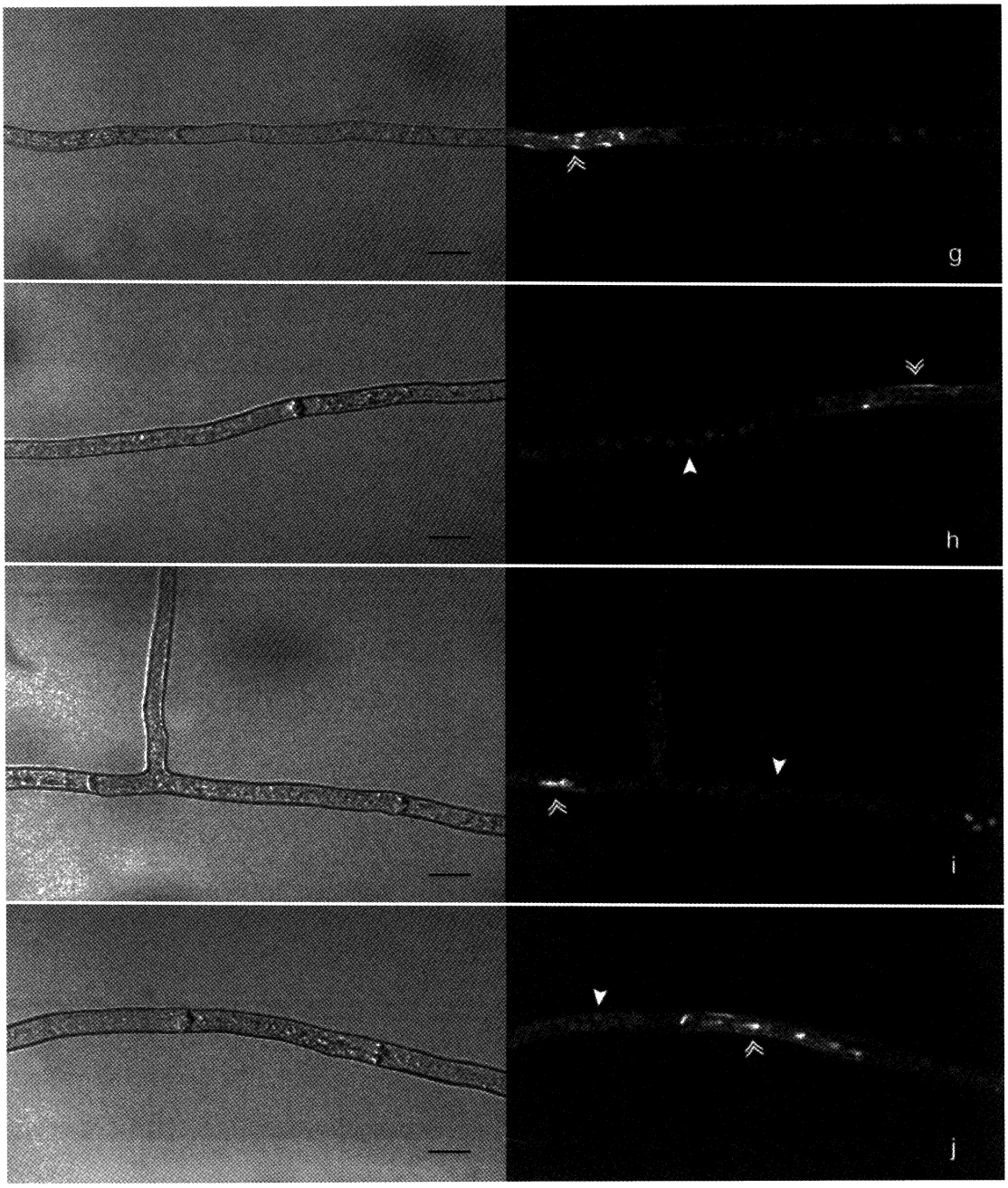

Fig. 5 a–j. In vivo 2PM of a partially septated, axenically cultured *G. rosea* specimen (specimen B). Transmitted-light (left) and 2PM (right) micrographs display cytoplasmic and nuclear features of different germ-tube zones. **a** Germ-tube apical zone displaying "clean septa" and, backwards, granularly vacuolated cytoplasm containing irregularly shaped, brightly fluorescent nuclei. **b–d** These cytological features are maintained some hundreds of micrometers along the hypha (towards the spore) (**b** and **c**) up to another clean-septa zone (**d**). **e** Higher magnification of the chromatin mass shown in **d** (double arrowheads) reveals its strand-like, particulate appearance. **f** After the clean-septa zone shown in **d**, a new cytoplasmic zone containing round, dim nuclei was found. **g** These features were maintained several hundreds of micrometers back towards the spore, up to a short clean-septa zone, after which a new cytoplasmic zone containing bright, irregularly shaped nuclei reappeared (double arrowheads). **h–j** Zones containing round, dim nuclei (solid arrowheads) alternate with others containing irregular, brightly fluorescent nuclei (double arrowheads) along the rest of the germ tube up to the spore. Both cytoplasmic zones are separated from each other by septa. Bars: a–d and f–j, 10 μm; e, 5 μm

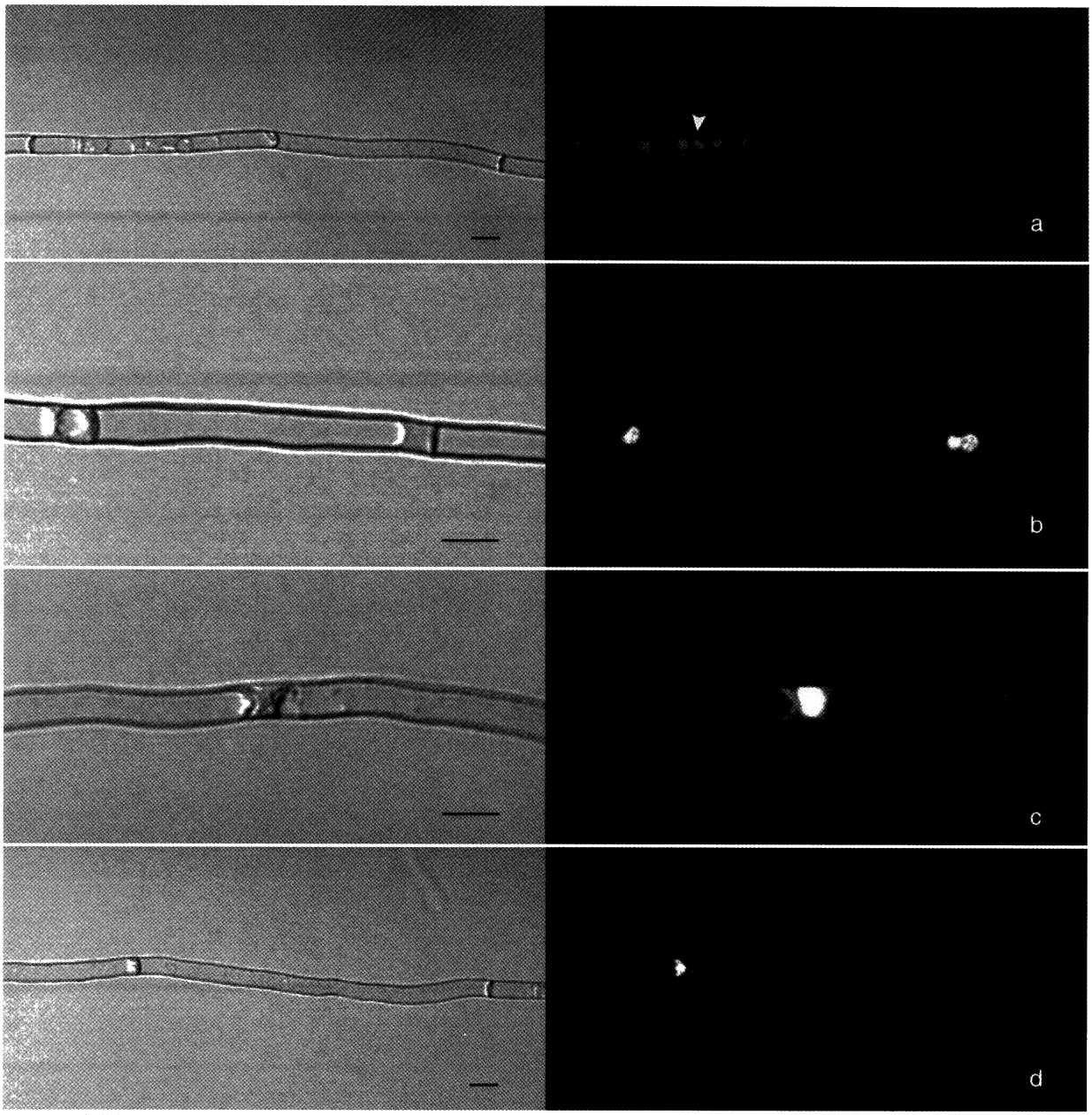

Fig. 6 a–d. In vivo microscopy of a fully septated, axenically cultured *G. rosea* specimen (specimen C). Transmitted-light (left) and 2PM (right) micrographs display cytoplasmic and nuclear features of different germ-tube zones. **a** A septated germ-tube zone still containing some remnants of vacuolated cytoplasm. Some round-shaped, dim nuclei are still evident (solid arrowhead). **b** Cytoplasm remnants between septa containing brightly fluorescent nuclei. **c** and **d** In some germ tubes the presence of brightly fluorescent chromatin debris squeezed between close "clean septa" is revealed. Bars: 10 μm

(Fig. 5 e). Small, isolated pieces of fluorescent material were also present.

The clean-septa germ-tube zone illustrated in Figs. 4 and 5 d extended several millimeters ending in a region in which cytoplasm reappeared displaying a more granular texture (Figs. 4 and 5 f, left) and containing nuclei which appeared roundish and dimmer than those described above (Fig. 5 f, right). These features were maintained for several hundreds of micrometers up to a short germ-tube clean-septa zone (Figs. 4 and 5 g, left), which was followed by another germ-tube area containing irregularly shaped, bright nuclei (Fig. 4; delimited in Fig. 5 g, h, right).

As shown in Figs. 4 and 5 h–j, the "cytoplasmic discontinuities" described above were present all along the rest of the specimen B germ tube: granular and/or vacuolated cytoplasmic zones, containing brightly fluorescent nuclei (either round-oval or irregularly shaped), alternated with zones showing less granular cytoplasm and containing round, dim nuclei. The two types of cytoplasmic zones were well delimited by septa, which seemed to separate different cytoplasmic states. Dim nuclei were more difficult to distinguish as observations were carried out in germ-tube areas closer to the spore (compare Fig. 5 h with i and j).

Specimen C (Fig. 6) consisted of an entirely septated *G. rosea* germ tube. Transmitted-light images revealed that most of the hyphal length of this specimen displayed "clean septa" (Fig. 6 a–d, left) and was devoid of nuclei (Fig. 6 a–d, right). Where remnants of highly vacuolated cytoplasm were found, some roundish, dim nuclei were noted (Fig. 6 a). Brightly fluorescent chromatin masses were also noted clustered between close septa. In some cases they were round, nuclei-like structures (Fig. 6 b), in others they appeared as compressed nuclear debris (Fig. 6 c, d).

Discussion

The multinucleated and coenocytic nature of AM fungi, and the almost complete lack of knowledge concerning their genetics and nuclear cycle have greatly hampered progress on the knowledge of the biology of these fungi, and of arbuscular mycorrhizal plants. Although interesting data concerning morphology, number, distribution, and ploidy level of AM fungal nuclei have been reported, the fact that all these studies were carried out on fixed specimens did not allow for an investigation of the nuclear behavior along hyphae and the final fate of nuclei.

Small fungal nuclei are more difficult to visualize with light microscopy than those of other organisms (Heath 1987). In this respect fluorescence microscopy proved more useful (Butt et al. 1989). A further step in cytological and nuclear research was accomplished with the development of CLSM, which allowed optical sectioning and 3- and 4-D reconstruction of images, with significantly better resolution and contrast (Czymmek et al. 1994, Pawley 1995). However, the inherent limitation of fluorescence microscopy (both conventional or CLSM) is that either the labeling and/or observation technique could perturb the viability of the cell (Arndt-Jovin and Jovin 1989). Multiphoton microscopy can limit the perturbation caused by observation and provides unique advantages in the study of living cells (Williams et al. 1994). Amongst the different DNA-specific probes, DAPI has been pointed out as the best choice for studying DNA-containing organelles (Heath 1987), and extensively used in nuclear studies on different specimens (Kapuscinski 1995) including AM fungi (Cooke et al. 1987; Bianciotto and Bonfante 1992, 1993). This fluorochrome presents a very high affinity for double-stranded DNA, attaching by electrostatic, noncovalent bonds to the minor grove of A-T rich sequences (Kapuscinski 1995). It is a highly sensitive (4–8 times higher than mithramycin; Coleman et al. 1981), small molecule (m.w. 350) which is readily taken up by living cells (Heath 1987, Butt et al. 1989). Being relatively resistant to fading (Butt et al. 1989), it allows longer continued observation of the specimen, and, apparently, does not affect cell viability when used at low concentrations (Coleman and Goff 1980, Toda et al. 1981), as we have also noted in our preliminary viability assays.

The use of 2PM and DAPI on axenic cultures of *G. rosea* has allowed us to carry out for the first time in vivo microscopy studies on AM fungi, and thus to obtain new data on the organization and distribution, behavior and fate of nuclei during the nonsymbiotic phase of this AM fungus.

Organization and distribution of nuclei along AM fungal germ-tubes

In mature, nonseptated axenically cultured *G. rosea* germ tubes, round or oval shaped nuclei were almost omnipresent along the hyphae. Bianciotto and Bonfante (1993) described round nuclei as usually located in the central part of hyhae, whereas elongated nuclei appeared mostly next to the cell wall. Our in vivo 2PM observations gives a step forward, revealing that oval nuclei are motionless and remain somehow "anchored" in lateral positions of the germ tube, whereas centrally located, round nuclei move along with the cytoplasmic streaming.

Preliminary genetic evidence has suggested the existence of different nuclear populations within single AM fungal spores (Sanders and Wiemken 1997). The first day after germination, some 800 nuclei migrate out of the spore to the growing germ tube (Bécard and Pfeffer 1993). One could, thus, envisage different specialized nuclei moving along the emerging germ tube (round, migrating nuclei) to specific locations according to a preprogrammed fungal growth sched-

ule, then becoming "anchored" (oval, motionless nuclei) and expressing, leading (and, eventually, differentiating) the germ-tube area under their control. This would mean that different fungal compartments ("cells") within coenocytic AM fungal germ tubes would indeed exist, even in the absence of physical barriers (septa). Further cytological and molecular research is needed to verify such hypothesis.

As in other fungi, the correct distribution of nuclei along *G. rosea* hyphae would probably require the existence of molecular "motors" to produce the correct nuclear movements, and "sensors" to monitor the actual position of nuclei in the hypha. The fungal cytoskeleton (comprising microtubules and F-actin) seems to be intimately involved in these processes (Heath 1994). Interestingly, Åström et al. (1994) observed that microtubules of axenically cultured *Glomus mosseae* (another AM fungus) were located both in the cortical and central parts of germ tubes, with nuclei positioned along the microtubule tracks. These authors suggested that nuclear distribution in AM fungal hyphae could be a microtubule-dependent process. Our in vivo, 2PM observations on movement and positioning of *G. margarita* nuclei along the germ tubes seem to further support such hypothesis.

Nuclear behavior following fungal growth arrest

Fluorescence microscopy, CLSM and 2PM observations revealed that some restricted zones of mature germ tubes of axenically cultured *G . rosea*, as well as extensive hyphal zones of specimens beginning to septate, showed clusters of brightly DAPI-stained chromatin quite often in irregular and/or strand-like shapes. Both, the high specificity of DAPI for DNA and the size of the stained irregularly shaped organelles, indicate that these objects are, in fact, deformed nuclei. Additional colocalization experiments utilizing both DAPI and the mitochondria-specific stain MytoTracker Green FM (Molecular Probes, Eugene, Oreg., U.S.A.) ruled out the possibility that these structures are other DNA-containing organelles (i.e., mitochondria) rather than nuclei (data not shown). Hyphal clusters containing distorted nuclei usually exhibited a highly vacuolated cytoplasm, and were delimited by septa which isolated them from the rest of the hypha. Neither cytoplasmic streaming nor nuclear movement were observed in these zones. Considered together, these features suggest that in these clustered areas autolytic processes were taking place owing to the lack of a symbiotic "switch on" signal or to a subsequent signal for fungal growth arrest, the fungus not having found a host root to colonize. This hypothesis is based on the following observations: (i) such clusters were never noticed in young, actively-growing germ tubes; (ii) absence of cytoplasmic streaming and high vacuolation are features commonly found in cellular autolytic processes (e.g., programmed cell death; Groover et al. 1997); (iii) most nuclei showed irregular shapes in these zones, sometimes appearing lobed, sometimes as chromatin strands or masses (similarly featured nuclei have been described in cells undergoing programmed cell death/apoptotic processes; Katsuhara and Kawasaki 1996, Groover et al. 1997); and (iv) the brighter fluorescence displayed by nuclei and irregularly shaped nuclei in these zones. Two possible explanations for the increased fluorescence are plasma membrane damage at the clustered areas, which allow an easier flow of the dye into the hyphal cytoplasm, or increased DAPI fluorescence due to autolytic processes. Increased DAPI fluorescence has been reported in nuclei of animal cells treated with agents known to induce apoptosis (Miller et al. 1997). This is apparently due to the breakdown of the supercoiling organization of chromatin, which would render the DNA molecule minor groove more accessible to DAPI. Similarly, an increase in DAPI fluorescence of apoptotic tobacco cells has been remarked by one of us (H. Chamberland pers. obs.).

Our results suggest that, if there is no host root to colonize, *G. rosea* undergoes autolytic processes simultaneously in different germ-tube zones. Such autolytic events are characterized by increased cytoplasmic vacuolation, immediate cessation of cytoplasmic streaming, nuclear disruption, and a rapid septation of the affected zone in order to limit damages. The presence of random autolysis has already been shown in other filamentous fungi (Fencl 1978), and was attributed to random and localized ageing events. Trinci and Righelato (1970) confirmed that in filamentous fungi autolysis is not a synchronous process throughout the entire hypha, but only in individual compartments. However, within a lysed compartment the breakdown of organelles is synchronous. The results provided here constitute the first evidence of a similar behavior in AM fungi, where growth arrest was so far thought to occur through cytoplasmic retraction and septa formation starting from the germ-tube apex and towards the spore (e.g., Mosse, 1962, Bonfante and Perotto 1995).

Whether these random autolytic events undergone by

asymbiotic *G. rosea* germ tubes are programmed (starting as a consequence of the lack of the symbiotic "switch on" signal) or not, remains to be elucidated. As discussed by Groover et al. (1997) the key aspect of programmed cell death is that the dying cell is itself participating actively in its cellular disassembly by an ordered and concerted set of actions. Programmed cell death has been already found throughout the animal and plant kingdoms (Ellis et al. 1991, Martin et al. 1994, Groover et al. 1997, Kosslak et al. 1997, Legrand 1997, Nooden et al. 1997), and more recently suggested to occur also in fungi (Umar and Vangriensven 1997, Jacobson et al. 1998). It is thought to be a selective mechanism that allows cells to survive only when and where they are needed (Alberts et al. 1994, Legrand 1997). More research is required to clarify its possible occurrence in AM fungi.

Fate of nuclei released after spore germination

In completely septated hyphae some remnants of chromatin appeared compressed between closely neighbouring septa. This suggests that at least a part of the nuclei coming out of the AM fungal spore after germination do not reenter it (as it was commonly thought), but remain in the septated hypha and eventually degrade. Thus, and since AM fungal spores present the capacity of multiple re-germinations (Hepper 1984, Bago 1990) one could think that the number of nuclei contained in a single spore would decrease with increased number of re-germinations. However, Bécard and Pfeffer (1993) found that although the number of nuclei in the spore declined markedly (by 800) one day after germination, it recovered slowly later, probably due to mitotic events, and almost reached its original value. Thus, the recovery of all nuclei released earlier seems not to be necessary for the newly dormant spore. These findings, however, raise interesting questions concerning the type of nuclei that are lost following spore germination and asymbiotic fungal growth arrest, for instance, do they all belong to similar populations (e.g., the "germination and finding of a host root" nuclear populations)? This would result in certain nuclear populations within a spore decreasing in number with respect to others. The development of adequate molecular biology tools allowing us to address this and other fundamental questions is indeed required.

It is well known that, in absence of soil disturbance, the AM fungal mycelium retains its colonization potential, even if hyphae are old and/or environmental conditions are adverse (Jasper et al. 1989). Warner and Mosse (1980) reported that some hyphae in the soil were still capable of colonizing plants even if detached of the original inoculum. Interestingly, our 2PM observations revealed that during the germ-tube septation process, and even in fully septated hyphae, cytoplasmic clusters containing normal-looking nuclei were present. It is tempting to associate such "forgotten" nuclei with the maintenance of the infectivity potential of AM fungal hyphae under natural conditions. Hopefully forthcoming research will clarify this point.

Acknowledgements

The authors gratefully acknowledge the technical support of Julie Samson (CRBF, U. Laval) and Kenneth Orndorff (Darmouth Medical School, Hanover, N.H., U.S.A.). Special thanks are due to François Larochelle, Maurice Lalonde and Alice Roy (CRBF, U. Laval). B. B. also duly acknowledges the faculty and colleagues of the 1st Course on 3-D Microscopy of Living Cells (Vancouver, 1996), and the financial assistance provided by Karl Zeiss Canada. This work has been supported by two postdoctoral fellowships to B. B. (Dirección General de Investigación Científica y Técnica, Spain, and Ministère de l'Éducation, Québec), as well as by NSERC research grants to Y. P. and J. G. L. and by NIH/NCCR funding of the Developmental Resource for Biophysical Imaging and Optoelectronics at Cornell University (W. Z., R. M. W., and W. W. W.).

References

Alberts B, Bray D, Lewis J, Raff M, Roberts K, Watson JD (1994) Molecular biology of the cell, 3rd edn. Garland Publishing, New York

Arndt-Jovin DJ, Jovin TM (1989) Fluorescence labeling and microscopy of DNA. Methods Cell Biol 30: 417–448

Åström H, Giovannetti M, Raudaskoski M (1994) Cytoskeletal components in the arbuscular mycorrhizal fungus *Glomus mosseae*. Mol Plant Microbe Interact 7: 309–312

Azcón-Aguilar C, Bago B (1994) Physiological characteristics of the host plant promoting an undisturbed functioning of the mycorrhizal symbiosis. In: Gianinazzi S, Schüepp H (eds) Impact of arbuscular mycorrhizas on sustainable agriculture and natural ecosystems. Birkhäuser, Basel, pp 47–60.

– Barea JM (1995) Saprophitic growth of AMF. In: Varma A, Hock B (eds) Mycorrhiza: structure, function, molecular biology, and biotechnology. Springer, Berlin Heidelberg New York Tokyo, pp 391–407

Bago B (1990) Efecto de distintos compuestos azufrados sobre el crecimiento independiente del hongo formador de micorrizas va *Glomus mosseae*. Master thesis, Universidad de Granada, Granada, Spain

– Vierheilig H, Piché Y, Azcón-Aguilar C (1996) Nitrate depletion and pH changes induced by the extraradical mycelium of the arbuscular mycorrhizal fungus *Glomus intraradices* grown in monoxenic culture. New Phytol 133: 273–280

Bago B, Bentivenga SP, Brenac V, Dodd JC, Piché Y, Simon L (1998) Molecular analysis of *Gigaspora* (Glomales, Gigasporaceae). New Phytol 139 (in press)

Balestrini R, Bianciotto V, Bonfante-Fasolo P (1992) Nuclear architecture and DNA location in two VAM fungi. Mycorrhiza 1: 105–112

Barea JM, Jeffries P (1995) Arbuscular mycorrhizas in sustainable soil plant systems. In: Varma A, Hock B (eds) Mycorrhiza: structure, function, molecular biology, and biotechnology. Springer, Berlin Heidelberg New York Tokyo, pp 521–560

Bécard G, Pfeffer PE (1993) Status of nuclear division in arbuscular mycorrhizal fungi during in vitro development. Protoplasma 174: 62–68

– Piché Y (1989) Fungal growth stimulation by CO_2 and root exudates in vesicular-arbuscular mycorrhizal symbiosis. Appl Environ Microbiol 55: 2320–2325

Bianciotto V, Bonfante P (1992) Quantification of the nuclear DNA content of two arbuscular mycorrhizal fungi. Mycol Res 96: 1071–1076

– – (1993) Evidence of DNA replication in an arbuscular mycorrhizal fungus in the absence of the host plant. Protoplasma 176: 100–105

Bonfante P, Bianciotto V (1995) Presymbiotic versus symbiotic phase in arbuscular endomycorrhizal fungi: morphology and cytology. In: Varma A, Hock B (eds) Mycorrhiza: structure, function, molecular biology, and biotechnology. Springer, Berlin Heidelberg New York Tokyo, pp 229–247

– Perotto S (1995) Strategies of arbuscular mycorrhizal fungi when infecting host plants. New Phytol 130: 3–21

Bonfante-Fasolo P, Berta G, Fusconi A (1987) Distribution of nuclei in a VAM during its symbiotic phase. Trans Br Mycol Soc 88: 263–266

Burggraaf AJP, Beringer JE (1989) Absence of nuclear DNA synthesis in vesicular-arbuscular mycorrhizal fungi during in vitro development. New Phytol 111: 25–33

Butt TM, Hoch HC, Staples RC, St Leger RJ (1989) Use of fluorochromes in the study of fungal cytology and differentiation. Exp Mycol 13: 303–320

Coleman AW, Goff LJ (1980) Applications of fluorochromes to pollen biology I: mithramycin and 4′,6-diamidino-2-phenylindole (DAPI) as vital stains and for quantitation of nuclear DNA. Stain Technol 60:145–154

– Maguire MJ, Coleman JR (1981) Mithramycin and 4′,6-diamidino-2-phenylindole (DAPI): DNA staining for fluorescence microspectrophotometric measurements in nuclei, plastids and virus particles. J Histochem 29: 959–968

Cooke JC, Gemma JN, Koske RE (1987) Observations of nuclei in vesicular-arbuscular mycorrhizal fungi. Mycologia 79: 331–333

Czymmek KJ, Whallon JH, Klomparens KL (1994) Confocal microscopy in mycological research. Exp Mycol 18: 275–293

Denk W, Strickler JH, Webb WW (1990) Two-photon laser scanning fluorescence microscopy. Science 248: 73–76

– Piston DN, Webb WW (1995) Two-photon molecular excitation in laser scanning fluorescence microscopy. In: Pawley JB (ed) Handbook of biological confocal microscopy. Plenum, New York, pp 445–458

Ellis R, Yuan J, Horvitz R (1991) Mechanisms and functions of cell death. Annu Rev Cell Biol 7: 663–698

Fencl Z (1978) Cell ageing and autolysis. In: Smith JE, Berry DR (eds) The filamentous fungi, vol 3, developmental mycology. Halsted Press, New York, pp 389–405

Gerdemann JW (1955) Relation of a large soil-borne spore to phycomycetous mycorrhizal infections. Mycologia 47: 619

– Nicolson JH (1963) Spores of mycorrhizal *Endogone* species extracted from soil by wet-sieving and decanting. Trans Br Mycol Soc 46: 235–244

Giovannetti M, Sbrana C, Avio L, Citernesi AS, Logi C (1994) Recognition and infection process, basis for host specificity of arbuscular mycorrhizal fungi. In: Gianinazzi S , Schüepp H (eds) Impact of arbuscular mycorrhizas on sustainable agriculture and natural ecosystems. Birkhäuser, Basel, pp 61–72

Groover A, De Witt N, Heidel A, Jones A (1997) Programmed cell death of plant tracheary elements differentiating in vitro. Protoplasma 196: 197–211

Heath IB (1987) Fluorescent staining of fungal nuclei. In: Fuller MS, Jaworski A (eds) Zoosporic fungi in teaching and research. Southeastern Publishing, Greenville, pp 169–171

– (1994) The cytoskeleton in hyphal growth, organelle movements and mitosis. In: Wessels JGH, Meinhardt F (eds) The Mycota, vol 1, growth, differentiation and sexuality. Springer, Berlin Heidelberg New York Tokyo, pp 43–65

Hepper C (1983) Limited independent growth of a vesicular-arbuscular mycorrhizal fungus in vitro. New Phytol 93: 537–542

– (1984) Isolation and culture of VA mycorrhizal (VAM) fungi. In: Powell CL, Bagyaraj DJ (eds) VA mycorrhiza. CRC Press, Boca Raton, pp 95–112

Jasper DA, Abbott LK, Robson AD (1989) Hyphae of vesicular-arbuscular mycorrhizal fungus maintain infectivity in dry soil, except when the soil is disturbed. New Phytol 112: 101–107

Jacobson DJ, Beurkens K, Klomparens KL (1998) Microscopic and ultrastructural examination of vegetative incompatibility in partial diploids heterozygous at het loci in *Neurospora crassa*. Fungal Gen Biol 23: 45–56

Kapuscinski J (1995) DAPI: a DNA-specific fluorescent probe. Biotech Histochem 70: 220–233

Katsuhara M, Kawasaki T (1996) Salt stress induced nuclear and DNA degradation in meristematic cells of barley roots. Plant Cell Physiol 37: 169–173

Kosslak RM, Chamberlin MA, Palmer RG, Bowen BA (1997) Programmed cell death in the root cortex of soybean root necrosis mutants. Plant J 11: 729–745

Legrand EK (1997) An adaptationist view of apoptosis. Q Rev Biol 72: 135–147

Marsh BAB (1971) Measurement of length in random arrangement of lines. J Appl Ecol 8: 265–267

Martin SJ, Green DR, Cotter TG (1994) Dicing with death: dissecting the components of the apoptosis machinery. Trends Biochem Sci 19: 26–30

Meier R, Charvat I (1992) Germination of *Glomus mosseae* spores: procedure and ultrastructural analysis. Int J Plant Sci 153: 541–549

Miller T, Beausang LA, Meneghini M, Lidgard G (1997) Death-induced changes to the nuclear matrix: the use of anti-nuclear matrix antibodies to study agents of apoptosis. BioTechniques 15 : 1042–1047

Mosse B (1959) The regular germination of resting spores and some

observations on the growth requirements of an *Endogone* sp. causing vesicular-arbuscular mycorrhizas. Trans Br Mycol Soc 42: 273–286

– (1962) The establishment of vesicular-arbuscular mycorrhiza under aseptic conditions. J Gen Microbiol 27: 509–520

– (1988) Some studies related to "independent" growth of vesicular-arbuscular endophytes. Can J Bot 66: 2533–2540

Nooden LD, Guiamet JJ, John I (1997) Senescence mechanisms. Physiol Plant 101: 746–753

Pawley JB (ed) (1995) Handbook of biological confocal microscopy. Plenum, New York

Sanders IR, Wiemken A (1997) The diversity of AM fungi and its ecological significance. In: 48th Annual Meeting of the American Institute of Biological Sciences, August 3–7, 1997, Palais des Congrès de Montréal, Montréal, Canada, p 120

Smith SE, Read DJ (1997) Mycorrhizal symbiosis. Academic Press, San Diego

Sward RJ (1981a) The structure of the spores of *Gigaspora margarita* I: the dormant spore. New Phytol 87: 761–768

– (1981b) The structure of the spores of *Gigaspora margarita* II: changes accompanying germination. New Phytol 88: 661–666

– (1981c) The structure of the spores of *Gigaspora margarita* III: germ-tube emergence and growth. New Phytol 88: 667–673

Toda T, Yamamoto M, Yanagida M (1981) Sequential alterations in the nuclear chromatin region during mitosis of the fission yeast *Schizosaccharomyces pombe*: video fluorescence microscopy of synchronous growing wild-type and cold-sensitive cdc mutants by using a DNA-binding fluorescent probe. J Cell Sci 52: 271–287

Trinci APJ, Righelato RC (1970) Changes in constituents and ultrastructure of hyphal compartments during autolysis of glucosa starved *Penicillum chysogenum*. J Gen Microbiol 60: 239–249

Umar MH, Vangriensven LJLD (1997) Morphogenetic cell death in developing primordia of *Agaricus bisporus*. Mycologia 89: 274–277

Viera A, Glenn MG (1990) DNA content of vesicular-arbuscular mycorrhizal fungal spores. Mycologia 82: 263–267

Warner A, Mosse B (1980) Independent spread of vesicular-arbuscular mycorrhizal fungi in soil. Trans Br Mycol Soc 74: 407–410

Watrud LS, Heithaus III JJ, Jaworski A (1978) Geotropism in the endomycorrhizal fungus *Gigaspora margarita*. Mycologia 70: 449–452

Williams RM, Piston DW, Webb WW (1994) Two-photon molecular excitation provides intrinsic 3-dimensional resolution for laser-based microscopy and microphotochemistry. FASEB J 8: 804–813

Xu C, Webb WW (1996) Measurement of two-photon excitation cross sections of molecular fluorophores with data from 690 to 1050 nm. J Opt Soc Am B 13: 481–491

– Zipfel W, Shear JB, Williams RM, Webb WW (1996) Multiphoton fluorescence excitation: new spectral windows for biological non-linear microscopy. Proc Natl Acad Sci USA 93: 10763–10768

Three-dimensional periodic cubic membrane structure in the mitochondria of amoebae *Chaos carolinensis*

Yuru Deng* and **Mark Mieczkowski****

Summary. Through computer simulation of images produced by the transmission electron microscope (TEM), we have identified three-dimensional periodic cubic membrane structures in giant amoebae (*Chaos carolinensis*) mitochondria. The cubic membranes are based on the highly curved three-dimensional periodic cubic surfaces, sharing the same geometry of mathematically defined periodic minimal surfaces. The double-membrane structures identified here divide space into three separate and convoluted subspaces. Specimen preparation, specifically the tendency to cut oblique sections, of this membrane crystal has added to the complexity of the resulting TEM projections and until now prevented researchers from recognizing them. It is the added complexity of the oblique sections, though, that allows us to match the TEM projection to a computer simulation of the same with confidence. In this study, formation of cubic membrane structures in amoeba mitochondria was found to be dependent on diet. The cubic structures only occurred in the absence of food, and disappeared in the presence of food, suggesting a structural adaptation and possible advantages for amoeba's survival in nature. The verification of mathematically well-defined structures in unfed amoeba mitochondria is also important to the understanding of the mitochondrial bioenergetics in relation to the topology of the inner membrane, where major cellular energy production as well as free-radical generation are taking place. This understanding may carry great impact upon human health as far as aging and age-related degenerative diseases are concerned, especially as mitochondrial disorders have been implicated in these processes.

Keywords: Mitochondrial inner membrane; Diet; Periodic cubic surface; Cubic phases; Computer simulation; Transmission electron microscopy.

Abbreviations: G gyroid; D double diamond; P primitive; TEM transmission electron microscopy; PCS periodic cubic surface.

*Correspondence and reprints: Wadsworth Center, Empire State Plaza, P.O. Box 509, Albany, NY 12201-0509, U.S.A.
**Present address: Westbrook, Connecticut, U.S.A.

Introduction

Mitochondrial inner membranes contain many requisite enzymes of oxidative phosphorylation as a major site of energy production in aerobic eukaryotic cells. Evidence shows that mitochondria also play crucial roles in other cellular mechanisms such as aging (Kalous and Drahota 1996), apoptosis (Richeter et al. 1996) and very likely as recognition organelles for various stress responses (Lai et al. 1996). Our understanding of the structure of mitochondria comes mainly from thin-section transmission electron microscopy (TEM) studies. Due to the variations of inner membrane morphologies and the difficulties of comprehending underlying three-dimensional (3-D) structure through the projected two-dimensional (2-D) TEM images, the meaning of morphological changes of mitochondria remains an enigma. Observations by means of the recently developed techniques of EM tomography (Mannella et al. 1994, 1997; Perkins et al. 1997) suggest that the mitochondrial compartmentation is more complex than that of the generally accepted model (Palade 1952, Sjöstrand 1953). An identified and characteristic 3-D structure of this organelle certainly will bring a more complete understanding of various mitochondrial functions.

The presence of strikingly complex patterns in some mitochondria of the giant amoeba *Chaos carolinensis* has been described by Pappas and Brandt (1959) but without a well-established structural analysis. Daniels and Breyer (1968) also reported that many mitochondria in starved amoebae have enlarged tubules aligned